Journal of Structural Geology 32 (2010) 1754–1767

Contents lists available at ScienceDirect

Journal of Structural Geology

journal homepage: www.elsevier.com/locate/jsg

Geomechanical integrity of sealing faults during depressurisation of the Statfjord Field

F. Cuisiat [a,*], H.P. Jostad [a], L. Andresen [a], E. Skurtveit [a], E. Skomedal [b], M. Hettema [b], K. Lyslo [b]

[a] Norwegian Geotechnical Institute, P.O. Box 3930 Ullevål Stadion, N-0806 Oslo, Norway
[b] Statoil, N-4035 Stavanger, Norway

ARTICLE INFO

Article history:
Received 5 March 2009
Received in revised form
7 January 2010
Accepted 8 January 2010
Available online 18 January 2010

Keywords:
Geomechanics
Production
Reservoir
Fault
Sealing integrity

ABSTRACT

In this paper the results of geomechanical analyses of fault behaviour at the Statfjord Field carried out as part of Statfjord Late Life Project are presented. The objective was to assess the sealing integrity of the horst structure between the Statfjord and Snorre fields during final depressurisation of the Statfjord Field. According to field pressure observations the Brent Fault is to date still acting as a pressure seal between the Brent Field and the Statfjord Field, despite the large present-day depressurisation of the Brent Field. These observations were used as a calibration and verification of the stress conditions that can be sustained without modifying the seal integrity of the fault. Based on the calculated stress changes in the horst structure which are equal to or less critical than the calculated present stress changes on the Brent Fault, it is concluded that the mechanical effects associated with the planned depressurisation of the Statfjord Field during its late life phase will not affect significantly the hydraulic resistance of the horst structure. A parametric study was conducted to investigate the sensitivity of the calculated stress changes to various input parameters for fault geometry and properties. The largest uncertainty relates to the peak shear strength of the fault (core) zone.

1. Introduction

In this paper the stress response of a major sealing fault to a planned reduction in reservoir pressure during production is analysed. The fault and the horst structure it bounds appear as sealing pressure boundaries between Statfjord and the neighbouring field, Snorre, in the Norwegian North Sea. In response to the operator's concern, the main focus of the study is to investigate the possibility to develop zones with shear or tensile failure during production, as such zones may be subjected to significant changes in hydraulic resistance.

As documented in the literature, fluid injection or fluid withdrawal can both induce active faulting in oil and gas reservoirs (Grasso, 1992). Re-activation of reservoir bounding faults can cause a loss of seal integrity (Wiprut and Zoback, 2000), and slip on active faults can also cause shearing of production wells (Maury et al., 1992) or wellbore instability during drilling (Willson et al., 1999).

The analyses presented in this paper are carried out within the context of Statfjord Late Life Project, which was started by the operator to increase gas recovery by reducing the reservoir pressure (Boge et al., 2005). In order to assess the stress response caused by this pressure reduction and the sealing integrity of the horst structure, geomechanical models have been constructed to predict production-induced stress changes during the final phase of field production.

A calibration of the numerical approach is performed by calculating the stress changes in the Brent Fault due to present depressurisation of the Brent Field. From field observations, the Brent Fault, which acts as a hydraulic barrier between the Brent Field and the Statfjord Field has not experienced any significant change in the hydraulic communication across it, despite the present pore pressure depletion of nearly 30 MPa at the Brent Field. In our approach, the maximum shear stress and minimum principal effective stress due to the present pore pressure reduction at the Brent Field, are used as an indicator of the stress condition that does not give significant change in the mechanical sealing integrity of the Brent Fault. It is then argued that the properties of the Brent Fault and horst are similar, such that the above stress condition for the Brent Fault can be extrapolated to the horst structure during the depressurisation phase planned for the Statfjord Field.

Two dimensional (2D) plane strain, geomechanical analyses are carried out by looking at characteristic 2D cross sections through a geological model of the area. It is considered that 2D analyses are sufficient as a first-order approximation, given the general geometry

* Corresponding author. Tel.: +47 22 02 31 55; fax: +47 22 23 04 48.
E-mail address: fabrice.cuisiat@ngi.no (F. Cuisiat).

0191-8141/$ – see front matter © 2010 Elsevier Ltd. All rights reserved.
doi:10.1016/j.jsg.2010.01.006

of the problem and uncertainties in some of the input data (see discussion in Section 2.1). The geomechanical analyses are performed using the numerical code Plaxis v 8.2 (2004). Plaxis is a finite element program specially developed for geomechanical applications. In order to apply Plaxis to reservoir-type problems, a user-defined poro-elastic constitutive model has been implemented into Plaxis in order to take into account the compressibility of the grains due to changes in pore pressure (i.e. the Biot effect), as well as the compressibility of the pore fluid in shales during undrained deformation.

A critical input in the analyses is the mechanical properties of faults. Based on results from laboratory experiments on intact and faulted material, as well as an estimation of clay content within fault planes, fault properties are suggested for the analyses. A key feature that controls the stress changes in a fault zone is the degree of drainage of the fault zone for the timescale considered. It is shown that for the actual production time histories, the fault core can be considered to be drained.

In light of the uncertainties related to geometries and geomechanical properties of fault zones, a parametric study is performed in order to identify the main parameters controlling shear and normal stress changes and therefore, the possibility of developing shear and tensile failure of the faults. Based on the results of the parametric study, a base case model of the Brent Fault is defined for geomechanical assessment of the structure.

1.1. Description of the Statfjord Field

The Statfjord Field is located in the Tampen area in the northern part of the North Sea, between the Brent and Snorre fields (Fig. 1 top right). The water depth in the area is about 150 m. The Statfjord Field is located in a large, faulted block, which is tilted towards the west and comprises a number of smaller, faulted compartments along its east flank. Towards the south west the field is bounded by the Brent Fault, and in the north east a horst structure marks the boundary with the Snorre field (Fig. 1 bottom). Within the Statfjord Field there are two reservoir units; the Brent Group at around 2500 m below mean sea level and the Statfjord Formation at a depth of around 2700 m below mean sea level. The two reservoirs are separated by the Dunlin Group, which consists mainly of shale.

The field can be separated into a relatively undeformed main field area and an eastern flank which is heavily deformed by rotational slide blocks. The main tectonic event in the area is related to

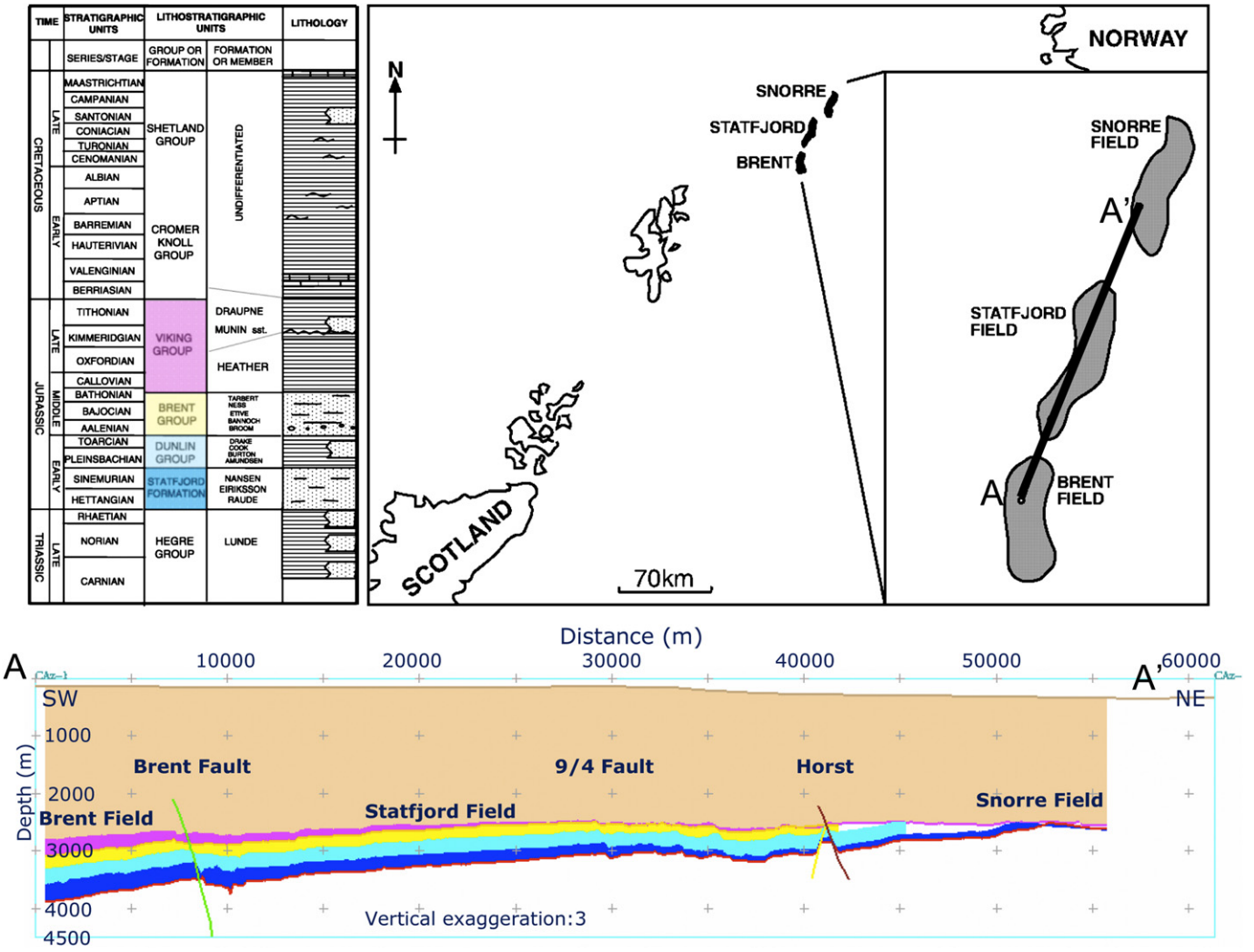

Fig. 1. Location of the Statfjord Field (top right). Regional stratigraphy of the Statfjord and Brent fields (top left). Global section (55 km wide) through the Statfjord Field including part of the Brent Field close to the Brent Fault, the horst structure and part of the Snorre field close to the horst structure (bottom). The section shows the seabed, Viking group (red), Brent group (yellow), Dunlin group (light blue) and Statfjord formation (dark blue). Vertical scale exaggerated by a factor of 3 compared to the horizontal scale. The Brent Fault between the Statfjord Field and the Brent Field and the Horst Structure between the Statfjord Field and the Snorre Field are highlighted. (For interpretation of the references to color in this figure legend, the reader is referred to the web version of this article.)

the opening of the Viking Graben which started in the Middle Jurassic. Subsequent deposition of the Draupne Formation caused gravitational instabilities along the crest of the field and the formation of rotationaly slide blocks in the Upper Triassic and Jurassic sections (Hesthammer et al., 1999).

1.2. Statfjord late life project

The Statfjord Late Life project started in 2005 in order to improve recovery from the Statfjord Field by converting the field from an oil field with associated gas, into a gas field with associated oil (Boge et al., 2005). This is achieved with a very extensive well programme, and modifications of the platforms and associated Tampen link pipeline to export gas. Gas export began in 2007. Production from the Statfjord Field is expected to continue until 2020.

The production strategy for the field was previously based on injecting gas and water for enhanced oil recovery and reservoir pressure maintenance. This resulted in over 60% crude oil recovery from the stock tank oil originally in place (STOOIP). In the late life phase of the field, the remaining non-recoverable oil is produced together with large volumes of previously-injected gas by reducing pressure in the reservoirs. A pressure reduction of about 30 MPa (300 bar) is planned, thereby reducing the pressure differences with the Brent Field, and inducing a large planned pressure drop through the horst connecting it with the Snorre field.

2. Description of numerical models

In this section, the basic elements of the numerical models are reviewed. The main input data to the geomechanical analyses consist of:

- Geometry (reservoir layers, fault structures, intra-reservoir shale layers, overburden and underburden)
- Initial vertical and horizontal stress, and pore pressure distribution
- Geomechanical properties (strength and stiffness) of intact, clay-rich materials (i.e. overburden, intra-reservoir shale layers, fault core)
- Geomechanical properties (stiffness and strength) of intact sand-rich materials (i.e. reservoir layers)
- Properties of faults (stiffness, strength and permeability)
- Pore pressure depletion histories
- Properties of fluid in place (fluid bulk modulus)
- Boundary conditions

2.1. Model geometry

The geometry of the geomechanical models is based on two-dimensional cross-sections through a geological model based on seismic data interpretation. Four different models were established: one global model and three local models (i.e. Brent Fault, horst structure and a simplified model of the Brent Fault for parametric studies). In the following, the geometry of the different models is reviewed.

The global model which is 60 km wide, extends from the Brent Field to the Snorre field. It is used to check the impact of boundary conditions in smaller local models around the faults considered (Fig. 2). The global model includes the Brent Fault separating the Statfjord Field and the Brent Field to the south-west, and the horst structure between the Statfjord Field and the Snorre field towards the northeast. The water depth varies from about 130 m in the south-west to 330 m in the northeast.

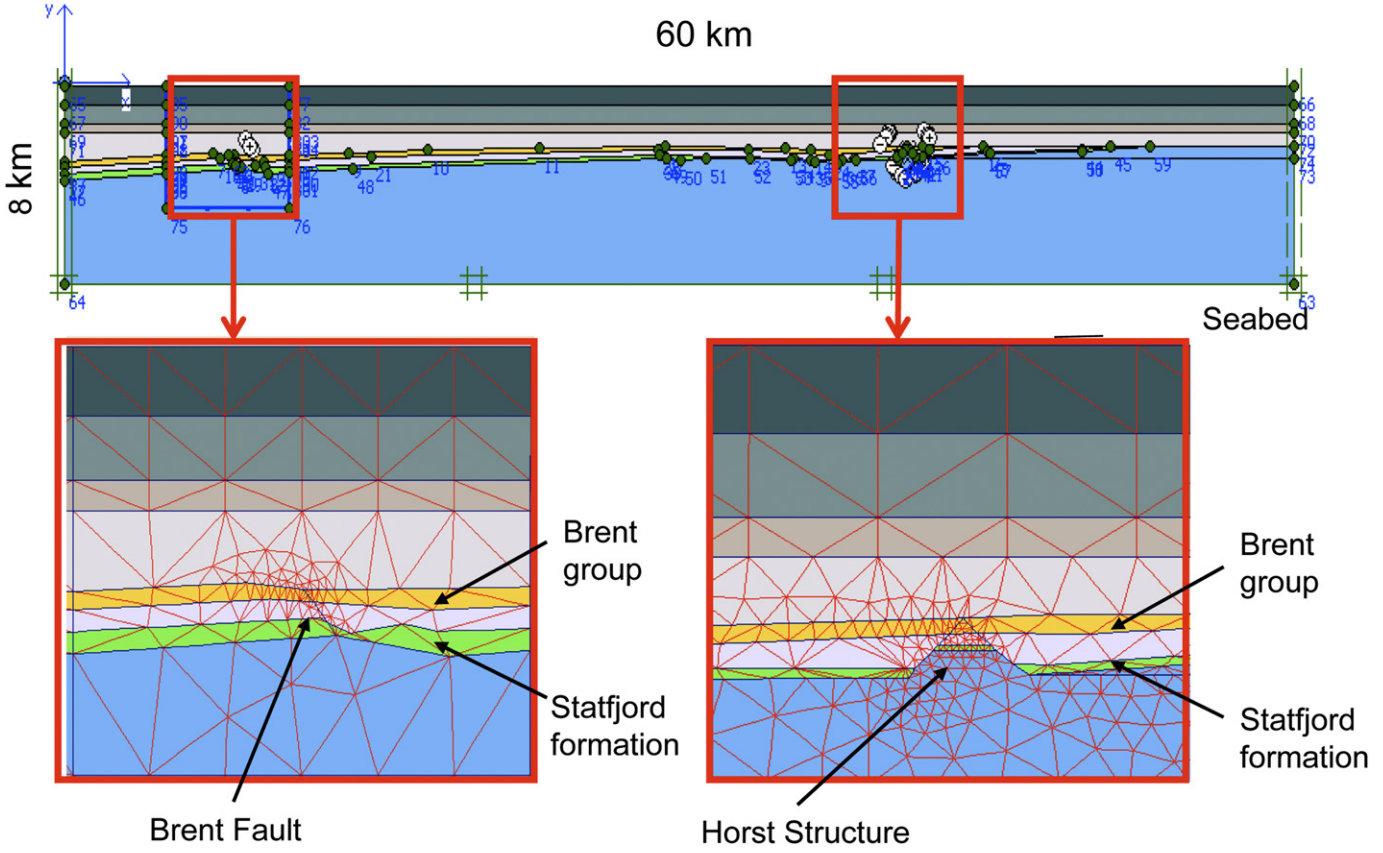

Fig. 2. Global 2D finite element model (top) with detail of the mesh around the Brent Fault (bottom left) and horst structure (bottom right).The Brent and Statfjord reservoirs are indicated on the figure.

Because of the variation in Brent Group thickness due to erosion and variation in fault dip along the strike of the fault, two vertical sections, Section 1 and Section 2, orientated roughly northeast–south-west through the Brent Fault, are considered. The main geometrical characteristics of the two sections are summarized in Table 1. The major difference between the two sections is the thickness of the Brent Group on the footwall side of the fault. In order to account for stiffness variation over the heights of the reservoir layers in the geomechanical model, the Brent Group is divided into two equally thick layers, Brent 1 (top) and Brent 2 (bottom). Similarly the Statfjord formation is divided into the Statfjord 1 (top) and Statfjord 2 (bottom), with thicknesses equal to 35% and 65% of the total unit thickness respectively. The finite element model used for Section 2 is illustrated in Fig. 3. A similar model to the Brent Fault model is used for the sensitivity study.

Three vertical sections orientated roughly north-east – south-west through the horst structure are used in the numerical analyses. The main differences between the three sections are the juxtaposition window of the Statfjord Formation across the fault zones and the thickness of the top Brent Group within the horst structure. For brevity, only data and results from Section 1 through the horst structure and illustrated in Fig. 4 are discussed in the paper. As for the Brent Fault model, the reservoir is divided into two layers due to variation in material properties with depth.

As shown in Figs. 3 and 4, simple planar fault geometries are assumed in this study. Furthermore, only two-dimensional plane strain models are used. This is considered reasonable given the general elongated geometry of the fields (NE–SW), which means that two-dimensional plane strain conditions should occur in the direction orthogonal to the elongated trend (i.e. roughly NW–SE and normal to the sections chosen for the analyses). The major assumptions underlying the models are justified by the following observations:

a) the fault is interpreted as being fairly planar along-strike at the scale considered here; in the absence of cross-cutting faults (i.e. parallel to chosen sections), stress variations in the out-of-plane are not expected and two-dimensional models can be used.
b) Three dimensional stress redistribution close to fault ends (along-strike) are not considered.
c) The behaviour of the faults and the general deformation mode are largely controlled by the global deformation of the compacting reservoirs (i.e. the driving forces), and the stiffness contrast between reservoirs and surrounding formations.

In fact, since the focus of the analyses is to study local stress conditions at the intersection of the faults and the elongated fields, the models should be regarded as two-dimensional cross-sections oriented normal to the fault planes. Hence, one can consider that locally the true fault orientation is transformed to be normal to the considered section, even though there might be some variation in fault orientation at a larger scale.

Table 1
Geometrical characteristic of two vertical sections through Brent fault used in two-dimensional numerical analyses.

	Section 1	Section 2
Average fault inclination (deg.)	54	47
Thickness of Brent Group Footwall – Hanging wall (m)	37–183	204–212
Thickness of Statfjord Formation Footwall – Hanging wall (m)	283–319	268–314

2.2. Initial stresses and pore pressures

The *in situ* stress conditions are characterized by a stress regime consistent with normal faulting, i.e. the vertical stress is the maximum principal stress. The stress regime is confirmed by the operator's drilling experience in the field. The minimum horizontal stress is obtained from extended leak-off tests (Raaen et al., 2006) and mini-fracture tests. There is no field evidence indicating large horizontal stress anisotropy; hence, the two horizontal stresses are assumed equal. Fig. 5 shows the total vertical stress, the total horizontal stress and initial pore pressure profiles as used in the geomechanical analyses. The hydrostatic pressure line is included for reference.

2.3. Material properties for overburden and surrounding shale

The overburden and surrounding shale formations are modelled as poro-elastic undrained material characterized by the following parameters:

- Shear modulus – G
- Drained Poisson's ratio – ν
- Bulk modulus of solid grains – K_s
- Porosity – n
- Fluid bulk modulus – K_f

The drained Poisson's ratio (ν) is taken equal to 0.2, i.e. representative of low porosity shales. In fact, the value has a limited effect in the analyses since, for shales, the excess pore pressure induced by volumetric deformation in undrained conditions is controlled by Skempton's coefficient B. The variation of B is small when ν varies between 0.1 and 0.3.

The bulk modulus of pore fluid (K_f) and solid (K_s) is taken to be 2.2 GPa (i.e. brine) and 45 GPa respectively. For simplicity, the shear modulus G is assumed to vary linearly from zero at seabed to a given value at the top of the reservoir; this is determined from the results of two undrained triaxial tests performed in NGI's soil and rock mechanics laboratory on Viking Group and Burton Formation shale core samples:

$$G = 0.8(D - 0.145) \tag{1}$$

where G is the shear modulus in GPa, and D is the true vertical depth below mean sea level (TVD msl) in kilometres. Note that Eq. (1) is field specific and not general for shales.

Eq. (1) gives a higher stiffness than the empirical model proposed by Horsrud (2001), which relates the Young's modulus E to the measured P-wave interval transit time Δt_p according to:

$$E = 0.076(304.8/\Delta t_p)^{3.23} \tag{2}$$

The discrepancy may be explained by the dataset used to establish Eq. (2), which is mostly based on younger, mechanically weaker Tertiary age shales from the North Sea.

2.4. Material properties for reservoir layers

The reservoir layers are modelled as drained, poro-elastic formations characterized by the shear modulus G, Poisson's ratio ν, and bulk modulus of the grains K_s. The drained bulk modulus of the rock (K) is expressed as:

$$K = 2G\frac{(1+\nu)}{3(1-2\nu)} \tag{3}$$

and Biot's coefficient α as:

$$\alpha = 1 - K/K_s \tag{4}$$

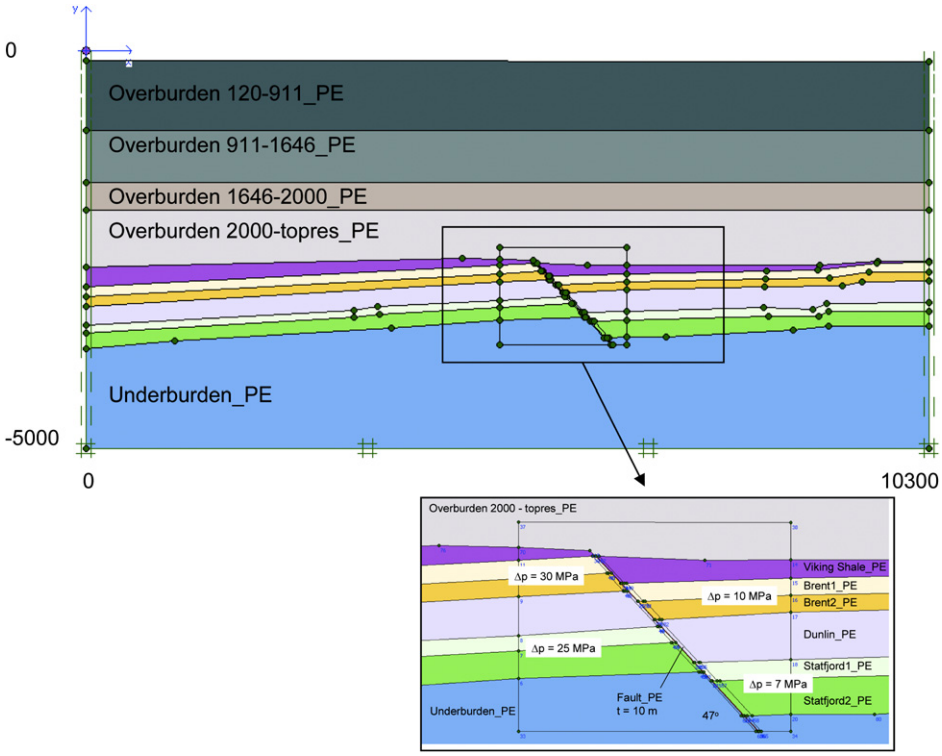

Fig. 3. Finite Element model of Brent Fault Section 2, with detailed view of reservoir section and fault.

The values of K, α, G and ν are inferred from triaxial tests performed in the laboratory on reservoir core samples. A nearly continuous core of some 720 m through the Brent and Dunlin Groups, and the Statfjord Formation was taken for rock mechanic studies. Special care was taken to minimise the damage caused by the coring process (Hettema et al., 2002). The interpreted values of the elastic properties are summarized in Table 2.

2.5. Properties of faults

In this section, the main geological characteristics of the faults are briefly presented, together with the approach used for modelling faults in the numerical analyses.

2.5.1. Fault geometry

The fault is defined by its throw, the fault core thickness, and the thickness of the damage zones on footwall and hanging wall sides (Sperrevik et al., 2002). Fault throw, inferred from seismic data, together with empirical correlations between damage zone thicknesses, fault core thickness and fault throw developed from outcrop studies (Beach et al., 1997, 1999), were used to estimate geometrical properties for the Brent Fault and the faults bounding the horst structure. These data are tabulated in Table 3 for two vertical sections through the Brent Fault and in Table 4 for one vertical section through the horst structure. In addition, the Shale Gouge Ratio (SGR) proposed by Yielding et al. (1997), which is a measure of the percentage of shale or clay in the slipped interval, is given in the tables.

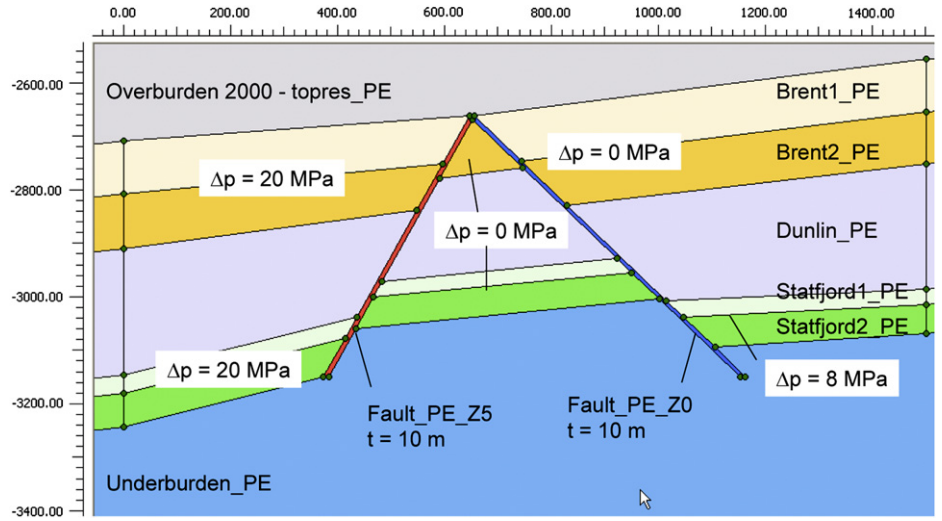

Fig. 4. Details of Finite Element model for horst structure Section 1. Note the faults "Z0" (Snorre side) and "Z5" (Statfjord side) defining the horst. Δp is the pressure reduction applied in the model.

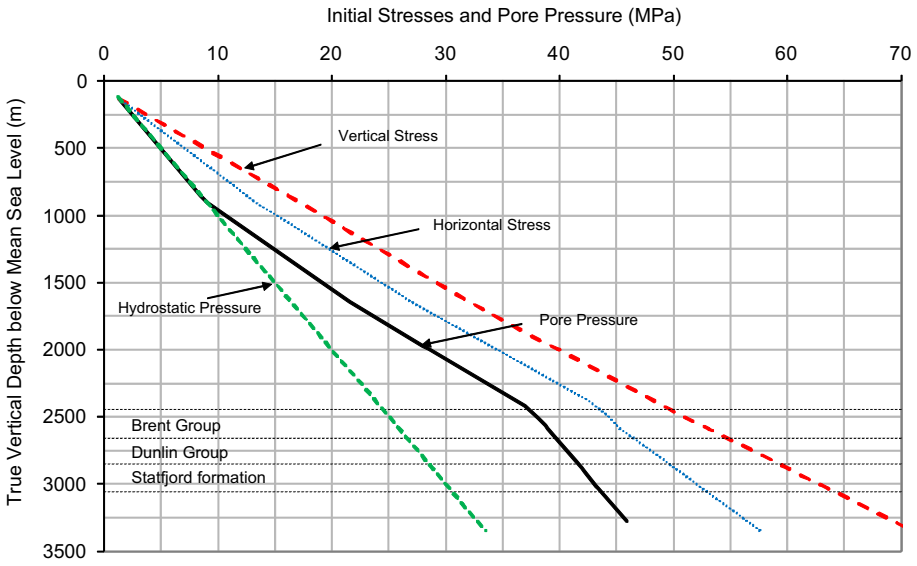

Fig. 5. Initial vertical and horizontal stresses and pore pressure for the Statfjord Field based on pore pressure prognosis, density logs, drilling experience, reservoir pressure measurements and mini-fracture tests (in the reservoir). The hydrostatic pressure line is included for reference. The depth in metres (vertical axis) is given as true vertical depth (TVD) below mean sea level.

Variation in the fault thickness is expected throughout the sandstone – shale sequence, with thicker damage zones observed in competent shale units than in sandstone units (Sperrevik et al., 2002). Significant "drag" of the adjacent layers to the fault due to shear deformation may also occur. However, in the absence of data related to the drag, in particular of the relationship between drag and fault throw, the drag component of deformation is not included in the "base case" numerical model. As shown later in a simplified parametric study, fault shear mobilisation is less when 'drag' effects are included, such that the base case is more conservative.

2.5.2. Fault mechanical properties

Shale Gouge Ratio (SGR) is used as an indication of the volume of clay within the fault plane. This is a simplification of fault zone complexity as SGR does not represent the detailed internal structure of a fault where clay smear, cataclasites, etc, might be present together (Wibberley et al., 2008). Table 3 indicates that for the Brent Group, the sand–sand juxtaposition window is sealed by a high clay concentration. Petrophysical and thin section analyses on fault rock material from the Brent Group reservoir show most fault rock may be classified as disaggregation zones/proto-cataclasites, indicating deformation at a relatively early stage in the reservoir's burial history (Sverdrup and Bjørlykke, 1997; Fisher and Knipe, 1998). In the Statfjord Formation, in view of the low SGR values in the sand–sand juxtaposition window (Table 3), it is assumed that the Brent Fault zone, which is acting as a seal, consists of a cataclastic fault rock, possibly with quartz cementation and higher shear strength. In the horst structure, due to high SGR values in the Statfjord Formation, low shear strength cannot be excluded (Table 4).

Table 2
Elastic properties of the reservoir layers inferred from over 100 triaxial tests on core samples from well 33/9-A-37b.

Formation/group	Porosity (%)	G (GPa)	ν (–)	K (GPa)	α
Upper Brent	27	3.7	0.21	5.1	0.86
Lower Brent	26	4.5	0.19	5.8	0.84
Upper Statfjord	25	4.4	0.21	6.1	0.83
Lower Statfjord	22	5.8	0.18	7.1	0.81

The shear strength of the clay-rich fault core zone is defined from the results of undrained triaxial tests carried out on core samples from Viking Group and Burton Formation shale. Due to limited data, a simple Mohr–Coulomb failure criterion is used. The drained peak shear strength is found to vary between lower and upper bounds as defined by the values of effective cohesion c' and friction angle φ' given by ($c' = 3$ MPa, $\varphi' = 24°$) and ($c' = 8$ MPa, $\varphi' = 23°$), respectively. The lower bound is obtained from specimens oriented at or close to the most critical orientation with respect to loading. From these tests, an average shear modulus G_{50} of 2.0 GPa is also found, which is used for the fault core zone (base case).

2.5.3. Modelling of faults in finite element models

Except for the global model, the fault is modelled with continuum elements having a finite thickness. In the global model the faults are represented with interface elements. The results from the parametric study show that stress changes on the fault are not very sensitive to fault core thickness. Hence a constant thickness of the fault core is used in the analyses despite the variation indicated in Tables 3 and 4. Similarly, the damage zones and geometrical drag effects are not taken into account as the parametric analyses show a relatively small and positive effect with respect to shear mobilisation of the fault.

Table 3
Characteristics of two sections of Brent fault through Brent Group, Dunlin and Statfjord Formations. Data for Section 1 is written in plain, data for Section 2 in bold letters (data from Statoil).

Formation/Group	Throw (m)	Fault zone thickness (m)	Damage zone thickness (m)	SGR
Brent 1	Eroded	Eroded	Eroded	Eroded
	140–160	**0.20–0.25**	**36**	**30–40**
Brent 2	155–165	0.20–0.30	40	40–50
	160–190	**0.25–0.35**	**50**	**30–50**
Dunlin	155–165	0.20–0.30	40	>50
	150–230	**0.20–0.40**	**32–60**	**>50**
Statfjord 1	155–165	0.20–0.30	40	<15
	190–245	**0.35–0.40**	**40–55**	**<15**
Statfjord 2	135–165	0.15–0.3	38–40	15–30
	245–260	**0.40–0.45**	**37–40**	**<15**

Table 4
Characteristics of Section 1 of horst structure through Brent Group, Dunlin and Statfjord Formation. Data for Fault Z0 is written in plain, data for Fault Z5 in bold letters. Data from Statoil.

Formation/group	Throw (m)	Fault zone thickness (m)	Damage zone thickness (m)	SGR
Brent 1	65–78	0.05–0.15	28	<35
	56–65	**0.05–0.10**	**24**	**10–25**
Brent 2	65–72	0.05–0.15	28	>35
	56–62	**0.05–0.10**	**24**	**25–50**
Dunlin	65–94	0.05–0.15	32	>50
	60–70	**0.10–0.15**	**30**	**>50**
Statfjord 1	91–94	0.05–0.15	32	>50
	60–78	**0.10–0.15**	**30**	**>40**
Statfjord 2	26–94	0.05–0.15	18–32	>50
	78–102	**0.10–0.20**	**32**	**>40**

2.5.4. Are faults drained or undrained during reservoir production?

A key feature that controls stress changes within the fault in response to pressure depletion in the reservoir sandstones is the consolidation behaviour of the fault, i.e. the ability for fluids within the fault to flow during the timescale investigated. This can lead to changes in pore fluid pressure within the fault. If the timescale is too short to allow fluid to flow, the stress changes in the fault zone are those associated with the undrained response of the medium. For a fluid-saturated, poro-elastic material, the relationship between stress and strain is equivalent to an ordinary elastic material with undrained mechanical parameters (Rice and Cleary, 1976). Such conditions can be, for instance, encountered in the evaluation of coseismic stress and strain changes within faults (Cocco and Rice, 2002). However, for reservoir depletion-induced stress changes, the timescale is usually in the order of decades. For instance, the pore pressure histories for the Brent Group and Statfjord Formation in this study show a pressure change over circa 25 years. For these long timescales, it is shown that the fault core is in a drained condition, given its permeability (albeit small) and thickness.

Let us consider the case where the fault is bounded by reservoir formations on hanging wall and footwall sides (i.e. sand–sand juxtaposition). Furthermore it is considered that from an initial condition, the reservoir pressure is reduced on one side only (Fig. 6). The permeability of the reservoir formations is much greater than that of the fault core material so that the reservoir formations can be considered fully-drained. In response to the pressure reduction, fluid flow takes place across the fault, and the fluid pressure within the fault evolves towards steady state flow conditions at a rate depending on fault thickness and fluid diffusivity (Fig. 6). Under steady state flow conditions, the pore pressure varies linearly across the fault (assuming uniform permeability within the fault).

The time before reaching almost 100% consolidation (i.e. steady state flow conditions) is given by:

$$t_{100} \approx L^2/c \quad (\mathrm{s}) \tag{5}$$

where L is the length of the drainage path, estimated to be about the thickness of the fault core zone, and c is the diffusivity (or consolidation coefficient; Rice and Cleary, 1976) given by:

$$c = \frac{k(K_u - K)(K + 4/3G)}{\mu_f \cdot \alpha^2 (K_u + 4/3G)} \quad \left(\mathrm{m}^2/\mathrm{s}\right) \tag{6}$$

where: k Intrinsic fault core permeability (m^2) K_u Undrained bulk modulus (MPa) K Drained bulk modulus (MPa) G Shear modulus (MPa) μ_f Dynamic viscosity (MPa s) α Biot coefficient.

The Biot coefficient is given by Eq. (4). The undrained bulk modulus can be inferred from the Biot–Gassmann relationship (Mavko et al., 1998; Hettema and de Pater, 1998) written as:

$$K_u = K + \frac{\alpha^2 K_s K_f}{nK_s + (\alpha - n)K_f} \tag{7}$$

where K_s is the bulk modulus of the solid grains constituting the fault core, K_f is the fluid bulk modulus and n the fault core porosity.

Fault core specimens are rarely available for specific offshore fields. In the absence of fault core material from the Statfjord Field, the results from laboratory measurements of permeability and diffusion coefficient on intact samples of Burton Formation shale (Dunlin Group) were used to estimate the consolidation time in the fault core. For a first-order estimate, an average of the four tests made parallel and normal to the lamination is used, disregarding the effect of anisotropy. This gives a permeability (k) and diffusivity coefficient (c) equal to 3.8×10^{-21} m^2 and 4.75×10^{-8} m^2/s (1.5 m^2/yr), respectively.

Assuming a fault core zone thickness between 0.2 m and 0.45 m, Eq. (5) gives t_{100} between 10 and 50 days. Hence, in view of the reservoir production timescale, segments of the fault core zone which juxtapose sand-rich reservoirs can be considered fully drained, with a pore pressure distribution through the fault (core) zone varying approximately linearly between the fluid pressures in the adjoining formations.

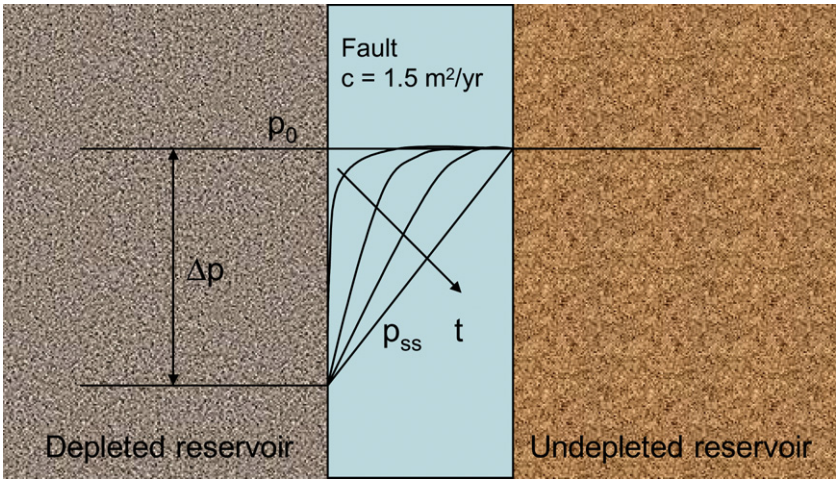

Fig. 6. Consolidation in a fault. The pressure in the reservoir on the left-hand side of the fault is depleted by Δp, while the pressure in the right hand side reservoir is unchanged. c is the diffusivity coefficient of the fault, t is time since depletion started, p_o the initial pressure and p_{ss} the steady state pressure distribution in the fault (i.e. at end of consolidation).

Table 5
Pore pressure reduction applied during modelling of the Brent fault (pressure histories for 2005).

Pressure reduction Δp (MPa)	Brent Field	Statfjord Field
Brent Group	30	8
Statfjord Formation	26	7

Table 6
Pore pressure reduction applied during modelling of the horst structure (pressure histories for year 2020).

Pressure reduction Δp (MPa)	Statfjord Field	Snorre Field
Brent Group	20	0
Statfjord Formation.	20	10

Note that t_{100} is inversely proportional to the permeability (k) of the fault core. The permeability of the fault core zone is highly uncertain, but a value much smaller than that of the intact shale is thought to be unrealistic. Even if the fault core permeability is ten times smaller than the value assumed above, the time to reach full consolidation (100–500 days) is still smaller than production time of several decades.

For sand–clay juxtaposition, i.e. for segments of the fault where the reservoir is juxtaposed to (undrained) shale-rich formations, it is assumed that the fault is fully drained, with pressure in the fault equal to the reservoir pressure.

2.6. Pore pressure history used for modelling

The pore pressure histories used in the study are obtained from history matched reservoir simulations using the black-oil reservoir simulation tool Eclipse™.

For modelling of the Brent Fault, pore pressure histories from 2005 (“present day situation”) are used. The resulting pore pressure reductions on both sides of the Brent Fault in the Brent Group and Statfjord Formation are given in Table 5. For modelling of the horst structure, pore pressure prognoses for the year 2020 (“Late life”) are considered. The resulting pore pressure reductions at both sides of the horst structure in the Brent Group and Statfjord Formation are given in Table 6.

The shale formation is assumed undrained during the depletion, i.e. no pore fluid flow takes place. The pore pressure distribution through the fault (core) zone is assumed to vary linearly between the pressures in the reservoir layer at both sides of the fault. The pore pressure in the damage zone is assumed to be equal to the pore pressure in the reservoir layer on the same side of the fault zone. The pore pressure within the horst structure is assumed to be constant during reservoir depletion.

2.7. Boundary conditions

Boundary conditions for all models are such that displacements along the bottom boundary are fully-fixed, the top boundary is free to move, while displacements along the side boundaries are fixed in the horizontal direction and free in the vertical direction.

3. Results from global analysis and parametric study

3.1. Global model

The global 2D model is used to assess the effects of boundary conditions in local models on the stress changes in the fault zone during depletion.

A comparison between a local and a global model shows that the displacement field is influenced by the close boundary conditions in a local model (Fig. 7). However, the shear and normal stresses along the fault are unaffected by the boundary conditions in the local model (Fig. 8). Hence, our local models may be used to study the stress changes in the fault during reservoir depletion, without significant effect of the close boundary conditions.

3.2. Parametric study of stress changes in fault core zone

The objective of the parametric study is to investigate the sensitivity of the stress response in a fault core zone to variations in fault geometry and material stiffness parameters. The two-dimensional finite element model used for the parametric analysis resembles the Brent Fault model (Section 2) at the Statfjord Formation depth.

From a base case scenario, variation of several parameters has been performed which can be grouped into:

- reservoir stiffness properties;
- overburden and intra-reservoir shale stiffness properties;
- fault geometry (inclination, thickness, drag and juxtaposition);
- pressure distribution and drainage of fault core zone.

The results presented in Table 7 are analysed in terms of maximum shear stress $\tau_{max} = (\sigma_1 - \sigma_3)/2$ and effective octahedral stress $\sigma'_{oct} = (\sigma'_1 + \sigma'_2 + \sigma'_3)/3$ in the critical location of the fault core zone. The results are averaged from the ten most critical integration points representing approximately 10 m of the fault length.

The closeness of the stress state to a Mohr–Coulomb failure line may be defined as the degree of shear mobilisation or *CF* (e.g. Templeton and Rice, 2008) given as:

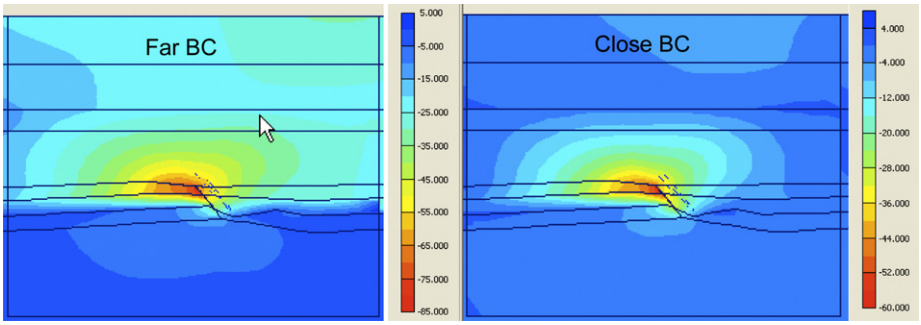

Fig. 7. Calculated contours of horizontal displacements (in centimetres) around the Brent Fault at Year 2005 (“Present day conditions”). Global 2D model (“Far BC”) and local model (“Close BC”). Note that color contours on the left and right figures have a slightly different scale.

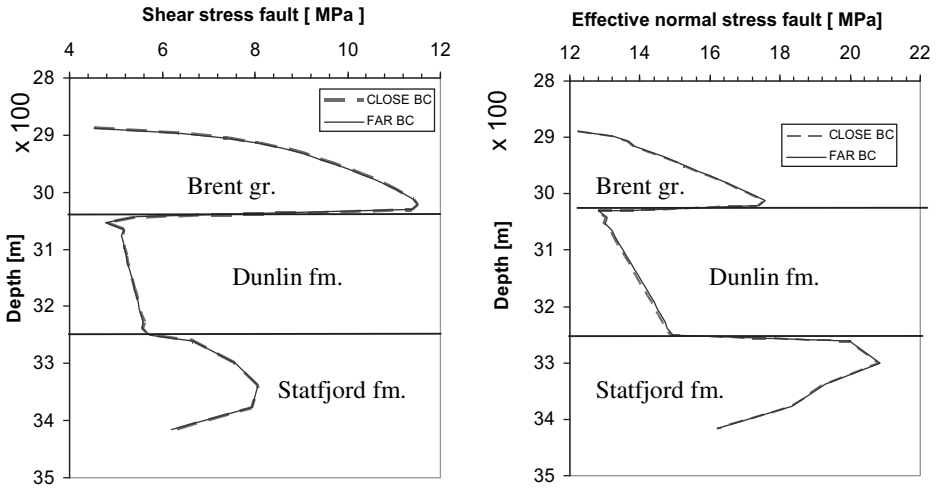

Fig. 8. Calculated effective normal and tangential (shear) stress along the Brent Fault (at the Brent Field side of the fault) at Year 2005. Global 2D model ("Far BC") and local model ("Close BC").

$$CF = \frac{\tau_{max}}{\sin\phi' \cdot (a + \sigma'_m)} \quad (8)$$

where $\sigma'_m = (\sigma'_1 + \sigma'_3)/2$ is the in-plane mean effective stress, a the attraction and ϕ' the effective friction angle of the fault core material. The attraction is related to the friction angle and the cohesion c' by $a = c'/\tan\phi'$. By using the values of cohesion and friction angle for clay/shale material presented in Section 2.5 ($c' = 3$ MPa, $\varphi' = 24°$), *CF* can be used to assess the positive or negative effect of varying one parameter with respect to shear mobilisation of the fault core. Note that the Mohr–Coulomb shear failure line corresponds to $CF = 1$. Since elastic analyses are performed (due to uncertainties in the strength parameters), values for *CF* in excess of 1 are possible.

Before depletion, τ_{max} and σ'_{oct} are related to the *in situ* effective vertical stress σ'_v and horizontal stress σ'_h by:

$$\begin{cases} \tau_{max} = \frac{1}{2}(\sigma'_V - \sigma'_h) \\ \sigma'_{oct} = \frac{1}{3}(\sigma'_V + 2\sigma'_h) \end{cases} \quad (9)$$

After reservoir depletion, the maximum shear stress in the fault core zone is concentrated in the area with sand–sand juxtaposition (Fig. 9); the most critical point being at the bottom of the depleted reservoir layer, except for a reverse fault (Case 12 in Table 7) where the most critical point is located at the top of the depleted reservoir. The degree of mobilisation (*CF*) increases from circa 0.6 to 1.3 (Base case) after depletion, indicating that shear failure may occur in the fault core zone. Note that the value of *CF* and the occurrence of shear failure depend on the actual shear strength. In fact, for the higher strength estimate, *CF* increases from circa 0.5 initially to 0.9 after depletion; this indicates no shear failure at all.

Table 7
Stress conditions at critical point in fault during reservoir depletion – results from parametric study. Figures in bold indicate an increase in shear stress mobilisation after variation of one input parameter from base case. E_{res}: Young's modulus of reservoir layers, ν_{res}: Poisson's ratio of reservoir layers, E_{shale}: Young's modulus of shale material, E_{fault}: Young's modulus of fault, *FZT*: fault zone thickness, L_{juxt}: Sand–sand juxtaposition length, β: fault inclination.

Case ID	Description	τ_{max} (MPa)	σ'_{oct} (MPa)	*CF*
	Initial conditions before depletion	6.7	16.6	0.64
1	*Base case* $E_{res} = 10$ GPa, $\nu_{res} = 0.2$, $E_{shale} = 4$ GPa, $E_{fault} = 4$ GPa, *FZT* = 10 m, $L_{juxt} = 50$ m, $\beta = 45°$	13.1	13.6	1.30
	Rock properties			
3	$E_{res} = 5$ GPa	13.7	15.6	1.25
5	$\nu_{res} = 0.4$	10.6	23.6	0.77
5b	$\nu_{res} = 0.1$	13.1	12.8	**1.35**
4	$E_{shale} = 8$ GPa	12.7	16.3	1.14
	Fault geometry and properties			
6	FZT = 20 m	12.6	14.0	1.24
7	FZT = 5 m	12.7	13.2	1.29
9	$E_{fault} = 8$ GPa	14.1	11.9	**1.49**
10	$\beta = 90°$ (vertical)	12.3	13.5	1.24
11	$\beta = 60°$	12.5	13.2	1.27
12	$\beta = -45°$ (reverse fault)	11.1	19.7	0.91
18	Presence of damage zones (thick = 20 m, $E_{damage} = 20$ GPa)	12.5	13.5	1.26
13	Reservoir juxtaposition $L_{juxt} = 100$ m	13.2	13.9	1.30
14	"Drag" of reservoir formations	11.9	16.7	1.07
	Pressure distribution			
2	Undrained fault	13.6	15.9	1.23
16	Fully depleted fault	15.5	23.9	1.06
17	Effect of differential pressure across the fault	18.0	15.9	**1.55**

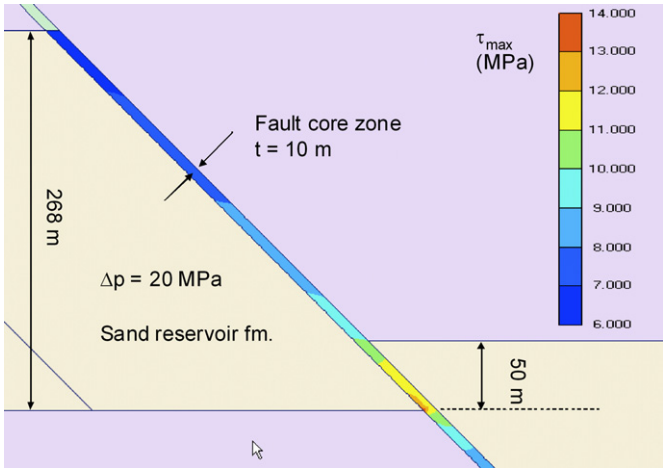

Fig. 9. Parametric study of maximum shear stress distribution in fault core zone. Base case result. Contours of maximum shear stress inside the fault core zone due to a 20 MPa pore pressure reduction in the footwall side of the fault. Maximum shear stress concentration occurs at the bottom of the 50 m sand–sand juxtaposition window.

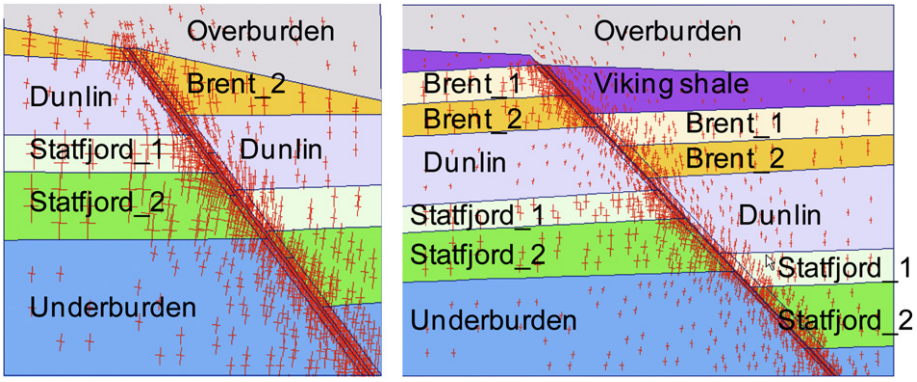

Fig. 10. Effective principal stresses (crosses) calculated at the year 2005 ("today's situation") around the Brent Fault for Section 1 (left) and Section 2 (right). Pore pressure reduction of 26 MPa (Statfjord formation) and 30 MPa (Brent group) in the Brent Field, of 7 MPa (Statfjord formation) and 8 MPa (Brent group) in the Statfjord Field. Note that the purpose of the figure is to illustrate principal stress re-orientation rather than stress magnitudes for which contour plots should be used. Hence no scale is linked to the crosses.

The maximum shear stress and effective octahedral stress changes in the fault core zone as calculated from the 2D analyses are relatively insensitive to variations in geometry and stiffness parameters. From the initial stress values of $\tau_{max,0} = 6.7$ MPa and $\sigma'_{oct,0} = 16.6$ MPa, the maximum shear stress and effective octahedral stress fall within a range $\tau_{max} = 12$–14 MPa and $\sigma'_{oct} = 12$–17 MPa after 20 MPa depletion for the majority of cases (Table 7). Furthermore, the parametric study shows that:

- The undrained behaviour of the fault core zone is less critical than a drained one (Case 2 versus Base case). Furthermore, as noted earlier, fully-drained behaviour is more relevant in view of production timescales and fault core permeability.
- The degree of shear mobilisation in the fault core zone is relatively insensitive to lower values of Poisson's ratio in the reservoir rocks (Case 5b), whereas higher values of Poisson's ratio lead to a reduction in shear mobilisation.
- The variation of fault core zone thickness (Cases 6 and 7) results in only minor stress changes, mostly due to slight difference in finite element discretization between the numerical models. This can be expected as long as the fault zone is very thin compared to the thickness of the reservoir layers and the fault stiffness is not significantly lower than the stiffness of the reservoir layers. The displacement field is then governed by the stiffness of the surrounding material rather than the fault properties. Hence, there is no significant consequence of using an unrealistic (e.g. too large) fault core zone thickness. Furthermore, the exact thickness of the fault core zone does not need to be known, and variations of the fault core zone width along the fault plane do not need to be modelled in detail.
- The potential for shear failure increases for a stiffer fault (Case 9).
- Fault dip (Cases 10–12) has a small effect on the fault stress response.
- Sand juxtaposition has little effect on the fault stress response and degree of shear mobilisation (Case 13).
- The effect of drag of reservoir formations along the fault plane (Case 14) is significant, but contributes to a decrease in the potential for shear stress mobilisation on the fault plane; hence it can be neglected for a first-order approach.
- When pore pressure changes in the fault core zone are considered (Case 16, with equal pore pressure in the depleted reservoir and the fault core zone), the degree of shear mobilisation mostly decreases due to an increase in the effective octahedral stress.
- The degree of shear mobilisation depends on the actual pore pressure history on both sides of the fault and not only on the pressure difference across the fault. This is illustrated by Case 17 where a differential pore pressure of 20 MPa is imposed, with a depletion of 30 MPa on the footwall side and a depletion of 10 MPa on the hanging wall side and in the fault core zone. This case, which is more critical than a depletion on only one side of 20 MPa, is also more realistic for the present day situation for the Brent Fault when compared to the Base case model.
- The presence of a stiffer damage zone (Case 18) represented with a constant thickness of 20 m and a Young's modulus twice as that of the reservoir sandstone, has a small positive impact on the degree of shear mobilisation. However, the consequence of damage zone and fault zone complexity for fluid behaviour, and the coupling between stress changes and hydraulic changes, is well-documented in the literature (e.g. Odling et al., 2004; Fisher and Knipe, 2001; Zhang and Sanderson, 1998). Assessing this is, however, beyond the scope of this study.

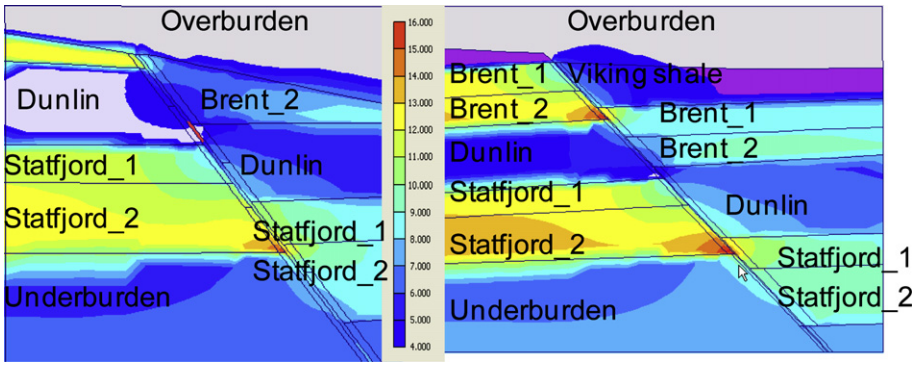

Fig. 11. Contours of maximum shear stress (4–16 MPa with increments of 1 MPa). Section 1 (left) and Section 2 (right) through the Brent Fault. Zones with shear stresses less than 4 MPa have no contours.

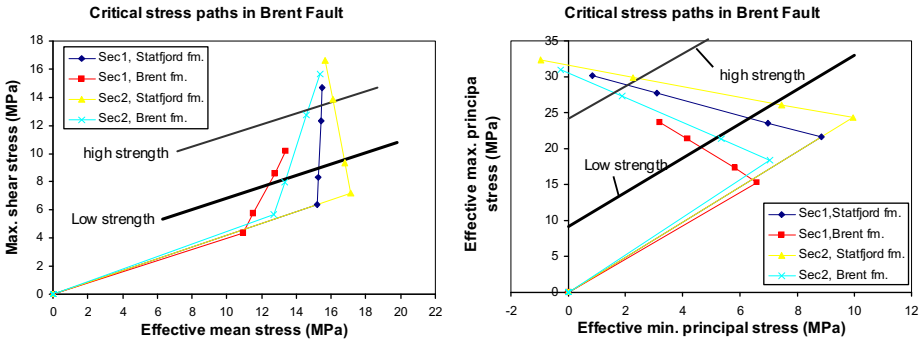

Fig. 12. Stress paths for critical points in Sections 1 and 2 through the Brent Fault. Effective mean stress vs. maximum shear stress (left) and minimum principal effective stress vs. maximum principal effective stress (right). Upper and lower bounds of shear strength are indicated for the Brent Group.

3.3. Shear- or tension-induced softening behaviour

The results of the parametric study show, during depletion of the reservoir, that the maximum shear stress in the fault core zone may reach the peak shear strength of the material constituting the fault core zone. Redistribution of maximum shear stress on the fault plane due to brittle softening may lead to propagation of failure zones along the fault. Similarly, propagation of tensile failure zones may occur due to effective minor principal stress softening (tension cut-off). These effects are analysed in two dedicated cases where; a) residual shear strength parameters ($\varphi_{res} = 15°$, $c_{res} = 3$ MPa) are introduced in a predefined area of the fault core zone and b) a Mohr–Coulomb model with tension cut-off $T = 0$ MPa is utilised. The details of the modelling are not presented here due to space limitation. The main conclusions from these two cases are: 1) if shear failure is initiated, the failure zone propagates along the fault dip direction rather than in the cross-fault direction and 2) if tension failure occurs it initiates on the non-depleted side of the fault core zone. Propagation of tension failure through the fault is not feasible because the fault is drained and the effective mean stress increases on the depleted side of the fault core zone. Furthermore, it is found that there is no significant tendency for a tension zone to propagate along the fault dip direction on the non-depleted side.

4. Stress conditions of the Brent Fault and horst structure

4.1. Present stress conditions of the Brent Fault

Fig. 10 shows the calculated effective principal stresses at the year 2005 around the Brent Fault in Section 1 (left) and Section 2 (right). There is little rotation of the principal stresses along the fault. The maximum shear stress after pressure reduction is equal to circa 16 MPa at the most critical points located in Section 2 at the bottom of the Statfjord Formation or Brent Group (Fig. 11 right, juxtaposition zones of Brent_2 to Brent_1 and Statfjord_2 to Statfjord_1). The corresponding maximum shear stress is about 10 MPa (Brent Group) and 14 MPa (Statfjord Formation) in Section 1.

The stress paths for two critical points in the fault core zone for both Section 1 and Section 2 are shown in Fig. 12, together with the upper and lower bounds for the peak shear strength of the shale. During pressure reduction in the reservoir, the critical point within the Brent Fault moves towards shear failure. Shear failure may be expected in the Brent Group as the shear failure criterion is exceeded, especially for the low shear strength estimate. Shear failure is less probable in the Statfjord Formation, although the modelling indicates stress levels in excess of the shear failure criterion. This is because the actual strength for the Statfjord Formation is probably significantly higher than the estimate plotted on the figure due to its low clay content and presumably cataclastic fault rock material. Tensile failure may also occur as indicated by the negative minimum principal stress (i.e. tensile stress) at the critical points in Section 2.

4.2. Stress conditions within the horst structure during the late life of the Statfjord Field

The results for the horst structure are shown for Section 1. This is found to be the most critical section investigated. Only the stress state at the end of production from the Statfjord Field (end of year 2020) is considered.

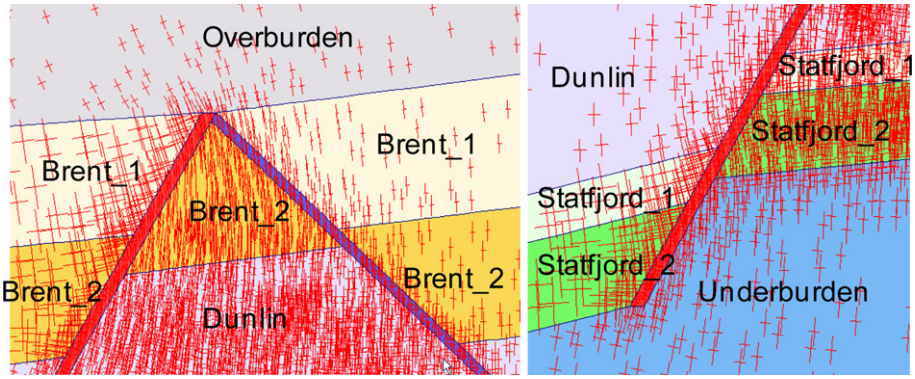

Fig. 13. Calculated effective principal stress crosses at the top of the horst structure (left) and at Fault Z5 in the juxtaposition of the Statfjord Formation (right) for Section 1. Note that the purpose of the figure is to illustrate principal stress re-orientation rather than stress magnitudes for which contour plots should be used. Hence no scale is linked to the crosses.

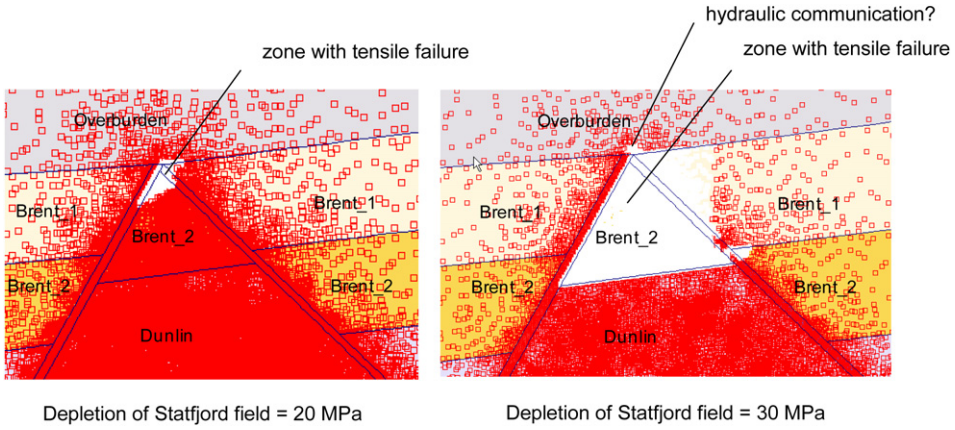

Fig. 14. Calculated zones with tensile stresses in Section 1 through the horst structure. Pore pressure depletion of 20 MPa (left) and 30 MPa (right) in the Statfjord Field side of the horst structure.

Fig. 13 (left) shows the calculated principal effective stress redistribution after pressure reduction at the top of the section through the horst structure. Fig. 13 (right) shows the same for Fault Z5 (Statfjord side of the horst), around the juxtaposition window of the Statfjord Formation (i.e. area where Statfjord_1 juxtaposes to Statfjord_2). Vertical tensile cracks may develop at the top sandstone within the horst structure, as the minimum effective principal stress is close to zero and its orientation is nearly horizontal. The extent of the zone with tensile stresses increases with the pore pressure depletion in the Statfjord Field (Fig. 14). The development of tensile stresses along the fault only occurs inside the horst structure. Tensile stresses are prevented from developing inside the fault towards the Statfjord Field due to the drained behaviour of the fault and effective stress increase during depletion. However, a zone with tensile stresses also develops from a singular point above the horst structure. In this area, a continuous drainage path would not be expected since tensile stresses are prevented from developing to the west of the horst structure (i.e. the depleted Statfjord Field side).

Stress paths for two critical points in Fault Z5 show that shear failure may occur in the Brent Group and the Statfjord Formation, as the low strength failure criterion is exceeded (Fig. 15). Tensile failure may also occur in the Brent Group as indicated by the negative minimum principal stress (i.e. tensile stress) at the critical points. The maximum shear stress is less than 10 MPa and concentrated in the juxtaposition windows (Fig. 16).

5. Discussion

5.1. Present stress conditions associated with the Brent Fault

Numerical analyses of the present (Year 2005) stress condition in the Brent Fault with significantly larger pore pressure depletion in the Brent Field compared to the Statfjord Field shows that shear failure may have occurred in the fault at the juxtaposition window for the Brent Group (i.e. Brent_2 against Brent_1 in Fig. 11). The peak shear strength in this zone is assumed to be similar to that of the Burton Formation shale, which is between 10 MPa and 18 MPa for an effective octahedral stress between 14 MPa and 20 MPa. This strength depends first of all on the orientation of the lamination compared to the orientation of the critical shear stress. The lowest strength is obtained when the critical stress is oriented parallel to the lamination. The actual orientation of the lamination within the fault core zones is, however, unknown.

As shown by the modelling, if shear failure occurs, it is initiated on the Statfjord Field side of the Brent Fault, i.e. the side with the lowest pore pressure depletion and thus also the lowest effective octahedral stress and corresponding strength. When the strength is reduced to the residual strength (strain softening), the failure zone may propagate along the fault but not across the fault. Tensile failure may occur on one side of the fault in areas of low effective horizontal stress (i.e. with the highest pore pressure). However, it cannot propagate across the fault zone due to the increased

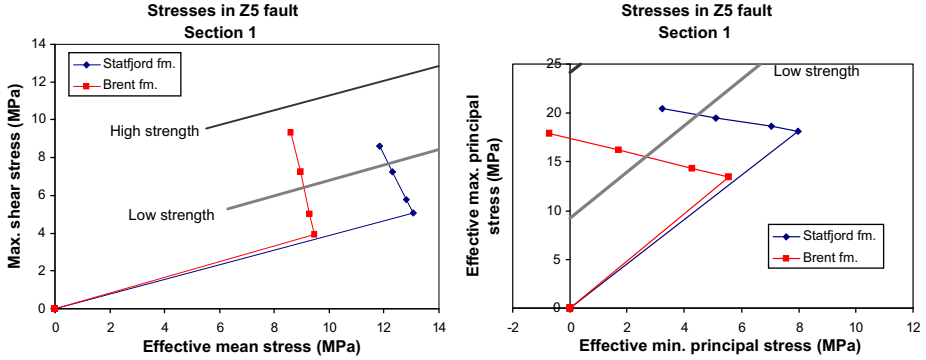

Fig. 15. Stress paths for critical points in Fault Z5, Section 1 through horst structure. Effective mean stress vs. maximum shear stress (left) and minimum principal effective stress vs. maximum principal effective stress (right). Upper and lower bounds of shear strength for the Brent Group are indicated.

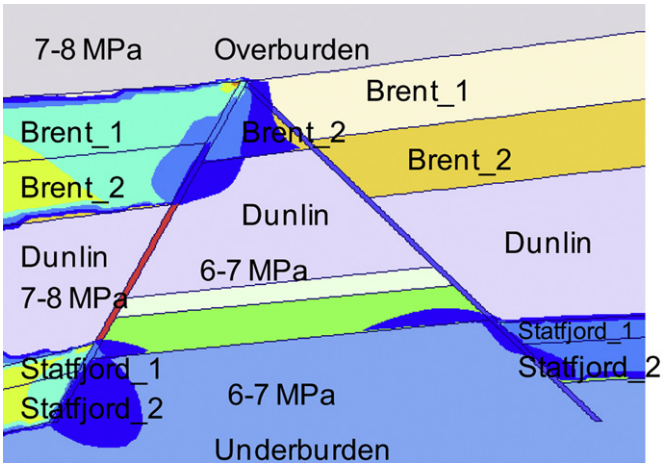

Fig. 16. Contours of maximum shear stress in MPa (from 6 to 12 MPa with increments of 1 MPa) for Section 1 through the horst structure at Year 2020 (Base Case). Areas with maximum values are indicated with figures and arrows.

effective horizontal stress on the other side (i.e. depleted side with the lowest pore pressure). Hence, a continuous zone with shear or tensile failure cannot develop across the fault core zone. As a result, only minor changes in hydraulic properties of the fault zone are expected as a result of present stress changes caused by pore pressure depletion on the Brent Field side. This conclusion agrees well with field observations, indicating no significant changes in the seal integrity of the Brent Fault, which currently acts as a hydraulic barrier between the Brent and Statfjord Fields.

5.2. Late life stress conditions on the horst structure

Analyses of the horst structure show similar stress changes in the fault zone between the Statfjord Field and the horst structure ("Fault Z5") as identified for the Brent Fault. However, the corresponding maximum shear stress in Fault Z5 is generally smaller than in the Brent Fault, such that the predicted late life stress situation is considered to be less critical than that already experienced by the Brent Fault. Hence, if mechanical and sealing properties for the two faults are similar, it can be concluded that the sealing integrity of the horst structure should not be altered significantly after full depletion of the Statfjord Field. Furthermore, the results of the modelling show that if failure takes place in the horst structure, then the failure zones (either shear or tensile failure) would propagate along and not across the fault (at the side with lowest or no depletion). The development of microcracks (and/or opening of pre-existing microcracks) is also inhibited on the depleted side of the horst structure (towards Statfjord) due to effective octahedral stress increase which occurs during depletion.

It should be pointed out that only mechanical effects due to effective stress changes were considered in this study. Other mechanisms (e.g. capillary effects) might contribute to change the hydraulic resistance of faults during pressure depletion.

6. Conclusions

We have presented the results of geomechanical analyses of fault behaviour at the Statfjord Field as part of Statfjord Late Life project. The objective was to assess the potential for developing hydraulic communication between the Statfjord and Snorre fields through a horst structure, during final depressurisation of the Statfjord Field. Two-dimensional plane strain geomechanical analyses were carried out to calculate the deformation and maximum shear stresses along the faults bounding the horst structure, resulting from compaction and horizontal deformation of the Statfjord Field due to pore pressure reduction.

The stress conditions at the Brent Fault separating the Brent and Statfjord Fields were first considered. According to pressure data, the fault is acting as a pressure seal between the two fields. The results of the modelling show that the calculated stress changes in the horst structure are equal to or less critical than the calculated present stress changes in the Brent Fault. It is therefore concluded that the mechanical effects (i.e. stress changes) associated with the planned depressurisation of the Statfjord Field during late life will not affect significantly the hydraulic resistance of the horst structure.

Only two-dimensional plane strain models and simple fault geometries were considered in this study, as the focus of the analyses was to identify failure modes and mechanisms rather than to predict absolute values of stress changes. The error by using a two-dimensional approach instead of three-dimensional modelling is less critical as the results are used quantitatively to compare two faults under similar conditions. This approach would not have been valid if the geometry of one fault had been very different to that of the other.

In light of the complexity and uncertainty associated with fault parameters, a parametric study was conducted to investigate the sensitivity of the modelled stress changes. This modelling can help to test several geological scenarios (e.g. presence of drag, thickness of fault) and assess the relative importance of particular mechanisms (e.g. drainage conditions). It is found that the maximum stress changes are not very sensitive to geometrical variations and uncertainties in stiffness distributions. The largest uncertainty relates to the peak shear strength of the fault (core) zone.

It should be pointed out that only the mechanical effects due to effective stress changes were considered in this study. Other mechanisms (e.g. capillary effects) might contribute to variations in the hydraulic resistance of faults during pressure depletion. Furthermore, the faults were modelled as single plane of weaknesses, which is clearly an over-simplification. Although the impact of damage zone was not properly modelled in this study, it was shown that its impact might not be so important for maximum shear stress distribution in the fault.

The integrity of the horst structure, as presented in this paper, was assessed relatively to the situation at the Brent Fault. Absolute predictions in terms of changes in hydraulic resistance were beyond the scope of this study. Further work would be required to develop petrophysical models which could relate the hydraulic properties of faults (e.g. permeability, capillary entry pressure) to mechanical changes (e.g. fault dilation, grain and pore volume, fracturing, tortuosity).

Instead, the approach chosen in this study assumed that the sealing conditions of the Brent Fault could be used to calibrate the methodology applied to the horst structure. This assumption is supported by geological understanding of the structures. However, the biggest uncertainty pertained to the strength of fault zones. Without specific fault data, but from expected clay content and deformation products in the fault zone, this study suggests that it is acceptable to use the residual shear strength of shales as representative of the strength of the fault (core) zone. Further work is required to improve the determination of the strength of faults. For instance, a systematic database could be developed by testing the strength, stiffness and hydraulic properties of fault core samples in the laboratory, for various fault deformation products sampled from core from offshore fields. In that way, reliable data for future analyses could be gathered.

Acknowledgements

The authors acknowledge the license partners of the Statfjord Field (Statoil, ExxonMobil, Shell, ConocoPhilips, Enterprise oil and Centrica) for their permission to publish this paper. We thank Rune Holt and Dave Dewhurst for reviewing the manuscript and contributing with valuable comments, and Chris Jackson for final editorial comments.

References

Beach, A., Brown, J.L., Welbon, A.I., McCallum, J.E., Brockbank, P.J., Knott, S.D., 1997. Characteristics of fault zones in sandstones from NW England: application to fault transmissibility. In: Meadows, N.S., Trueblood, S.P., Hardman, R., Cowan, G. (Eds.), Petroleum Geology of the Irish Sea and Adjacent Areas. Geological Society, London, Special Publications, vol. 124, pp. 315–324.

Beach, A., Welbon, A.I., Brockbank, P.J., McCallum, J.E., 1999. Reservoir damage around faults: outcrop examples form the Suez rift. Petroleum Geoscience 5, 109–116.

Boge, R., Lien, S.K., Gjesdal, A., Hansen, A.G., 2005. Turning a North Sea Oil Giant into a Gas Field – Depressurization of the Statfjord Field SPE 96403, Offshore Europe, 6–9 September, Aberdeen, United Kingdom.

Cocco, M., Rice, J.R., 2002. Pore pressure and poroelasticity effects in Coulomb stress analysis of earthquake interactions. Journal of Geophysical Research in Solid Earth 107, 2030.

Fisher, Q.J., Knipe, R.J., 1998. Fault sealing processes in siliciclastic sediments. In: Jones, G., Fisher, Q.J., Knipe, R.J. (Eds.), Faulting, Fault Sealing and Fluid Flow in Hydrocarbon Reservoirs. Geological Society, London, Special Publications, vol. 147, pp. 117–134.

Fisher, Q.J., Knipe, R.J., 2001. The permeability of faults within siliciclastic petroleum reservoirs of the North Sea and Norwegian Continental Shelf. Marine and Petroleum Geology 18, 1063–1081.

Grasso, J.R., 1992. Mechanics of seismic instabilities induced by the recovery of hydrocarbons. Pure and Applied Geophysics 139, 507–534.

Hesthammer, J., Jourdan, C.A., Nielsen, P.E., Ekern, T.E., Gibbons, K.A., 1999. A tectonostratigraphic framework for the Statfjord Field, northern North Sea. Petroleum Geoscience 5, 241–256.

Hettema, M.H.H., de Pater, C.J., 1998. The poromechanical behaviour of Felser Sandstone stress – and temperature-dependent SPE/ISRM 47270, SPE/ISRM Rock Mechanics in Petroleum Engineering, 8–10 (July, Trondheim, Norway).

Hettema, M.H.H., Hanssen, T.H., Jones, B.L., 2002. Minimizing Coring-Induced Damage in Consolidated Rock. SPE/ISRM 78156, SPE/ISRM Rock Mechanics Conference, 20–23 October, Irving, Texas.

Horsrud, P., 2001. Estimating mechanical properties of shale from empirical correlations. SPE 56017. SPE Drilling and Completion 16, 68–73.

Maury, V.M.R., Grasso, J.R., Wittlinger, G., 1992. Monitoring of subsidence and induced seismicity in the lacq gas-field (France) – the consequences on gas-production and field operation. Engineering Geology 32, 123–135.

Mavko, G., Mukerji, T., Dvorkin, J., 1998. The Rock Physics Handbook. Tools for Seismic Analysis in Porous Media. Cambridge University Press.

Odling, N.E., Harris, S.D., Knipe, R.J., 2004. Permeability scaling properties of fault damage zones in siliclastic rocks. Journal of Structural Geology 26, 1727–1747.

Plaxis User's Manual. Plaxis 2D Prof. v.8.2, Build 811, 2004. www.plaxis.nl.

Raaen, A.M., Horsrud, P., Kjorholt, H., Okland, D., 2006. Improved routine estimation of the minimum horizontal stress component from extended leak-off tests. International Journal of Rock Mechanics and Mining Sciences 43, 37–48.

Rice, J.R., Cleary, M.P., 1976. Some basic stress-diffusion solutions for fluid-saturated elastic porous media with compressible constituents. Reviews of Geophysics and Space Physics 14, 227–241.

Sperrevik, S., Gillespie, P.A., Fisher, J.F., Halvorsen, T., Knipe, R., 2002. Empirical Estimation of Fault Rock Properties. In: Norwegian Petroleum Society (NPF) Special Publication, vol. 11 109–125.

Sverdrup, E., Bjørlykke, K., 1997. Fault properties and the development of cemented fault zones in sedimentary basins: field examples and predictive models. In: Møller-Pedersen, P., Koestler, A.G. (Eds.), Hydrocarbon Seals: Importance for Exploration and Production. Norwegian Petroleum Society (NPF) Special Publications, vol. 7, pp. 91–106.

Templeton, E.L., Rice, J.R., 2008. Off-fault plasticity and earthquake rupture dynamics: 1. Dry materials or neglect of fluid pressure changes. Journal of Geophysical Research 113, B09306.

Wibberley, C.A.J., Yielding, G., Di Toro, G., 2008. Recent advances in the understanding of fault zone internal structure: a review. In: Wibberley, C.A.J., Kurz, W., Imber, J., Holdsworth, R.E., Collettini, C. (Eds.), The Internal Structure of Fault Zones: Implications for Mechanical and Fluid-Flow Properties. Geological Society, London, Special Publications, vol. 299, pp. 5–33.

Willson, S.M., Last, N.C., Zoback, M.D., Moos, D., 1999. Drilling in South America: a wellbore stability approach for complex geologic conditions SPE 53940, Latin American and Caribbean Petroleum Engineering Conference, 21–23 April, Caracas, Venezuela.

Wiprut, D., Zoback, M.D., 2000. Fault reactivation and fluid flow along a previously dormant normal fault in the northern North Sea. Geology 28, 595–598.

Yielding, G., Freeman, B., Needham, D.T., 1997. Quantitative fault seal prediction. American Association of Petroleum Geologists Bulletin 81, 897–917.

Zhang, X., Sanderson, D.J., 1998. Numerical study of critical behaviour of deformation and permeability of fractured rock masses. Marine and Petroleum Geology 15, 535–548.